

Stochastic Model for the Interaction of Buckling and Fracture in Thin Tension-Loaded Sheets

Bjørn Skjetne,^{1,2} Torbjørn Helle,¹ and Alex Hansen²

¹*Department of Chemical Engineering, Norwegian University of Science and Technology,
N-7491 Trondheim, Norway*

²*Department of Physics, Norwegian University of Science and Technology,
N-7491 Trondheim, Norway*

(Dated: November 19, 2018)

We introduce a model of fracture which includes the out-of-plane degrees of freedom necessary to describe buckling in a thin-sheet material. The model is a regular square lattice of elastic beams, rigidly connected at the nodes so as to preserve rotational invariance. Fracture is initiated by displacement control, applying a uniaxial force couple at the top and bottom rows of the lattice in mode-I type loading. The approach lends itself naturally to the inclusion of disorder and enables a wide variety of fracture behaviours to be studied, ranging from systems with a simple geometrical discontinuity to more complex crack geometries and random cracking. Breakdown can be initiated from a pre-cracked sheet or from an intact sheet where the first damage appears at random, and buckling sets in when a displacement vector containing out-of-plane components becomes energetically favourable over one which does not. In this paper we only consider center-cracked sheets with no disorder and include some results relevant to the force- and displacement-fields, and the buckling response ratio. Rather than carry out a comprehensive study of such systems, the emphasis presently is on the development of the model itself.

PACS numbers: 81.40.Jj, 62.20.-x, 05.40.-a

I. INTRODUCTION

Understanding how, and when, materials break are important in many engineering applications. This is so for a number of reasons – the motivation to study fracture may, for instance, be related to safety issues, such as determining when cracks form in concrete structures, or it may be one of economical gain, as in the case when the runnability of a printing press in the paper industry is considered. Few materials, be they natural or manufactured, are perfect, however. Hence, the disorder in the micro-structure needs to be accounted for in order to obtain a realistic description.

Over the past fifteen years methods have emerged within the statistical physics community to successfully tackle just such problems [1]. These methods are intermediate between the microscopic, or first principles, approach and the mean-field type of approach. In the former case fracture properties are derived from inter-molecular or inter-atomic forces, representing a problem which is both theoretically demanding and heavy on numerical resources. In the latter case disorder cannot be included in a satisfactory way. This is a big drawback since the presence of disorder in a material is crucial to the way it fractures. Disorder affects the stress field in such a way as to enhance the already existing heterogeneities. This interplay, between a constantly evolving non-uniform stress field and local variations in material properties, can nevertheless be handled in a numerically tractable way using lattice models.

The most common lattice models used in engineering applications are finite element methods (FEM), the implementation of which is usually based on commer-

cially available computer codes. The lattice models currently used in statistical physics differ somewhat from the FEM-approach in that the grid used is regular, i.e., the same everywhere, rather than one which adjusts the mesh size according to where the stress field is most intense. Although FEM modeling is certainly more suitable in describing homogeneous materials, the requirement that the stress field should vary slowly over each element makes the approach cumbersome in the presence of heterogeneities. In the stochastic lattice model, however, the nodes are thought of as being connected by objects such as elastic beams or current carrying elements. While in some respects being less sophisticated than FEM methods, the interpretation of the algorithm is much more transparent and the approach also has the advantage of allowing disorder to be included quite generally.

In the stochastic models, the local equilibrium in force and moment is considered on a mesoscopic scale, i.e., on a scale much smaller than the external dimension of the lattice but still sufficiently large for the forces to be governed by well known physical laws. In this sense it is also a very good alternative to the far more complicated approach of including disorder on the microscopic level. Since only the nearest neighbours on the lattice are included the calculation of the displacement field reduces to the inversion a sparse matrix, enabling reasonably large systems to be handled computationally.

One feature which is of a phenomenological nature, however, is the breaking rule – the choice here is guided by intuition rather than by the inner workings of the model itself. In other words, breaking does not arise as a natural consequence of the calculations. This is actually

an advantage in that the mechanism by which the system ruptures can be tailored to suit different engineering requirements. If we regard thin planar materials, for instance, the energy required to propagate a crack across a given area is usually much lower in mode-III fracture, i.e., tearing, than in the pure tensile loading of mode-I fracture. Familiar examples of disordered materials which behave this way are textiles and paper.

Most of the research done so far in stochastic lattice modeling aims to identify the underlying general principles of the fracture process rather than to address traditional problems in fracture mechanics. In this paper the plane beam model [2], which has been used previously to study scaling laws in fracture, is extended to include a specific, and practical, aspect of fracture which is very important for thin sheet materials, i.e., buckling. As is well known, buckling can profoundly influence the residual strength of such materials [3, 4, 5]. But before devoting our attention to this problem in full, we briefly mention part of the background which has inspired the use of lattice modeling as a tool in statistical physics.

In modeling experiments of random media, the feature which by far has received the most attention is the morphology of crack surfaces. Many surfaces in nature are found to be self-affine, i.e., statistically invariant with respect to anisotropic scale transformations. The morphology of such surfaces can be described by simple scaling laws, behaving very much like fractal objects [6]. These scaling laws provide a theoretical framework whereby much information can be summed up in a few parameters. Certain features have been found to share a common basis with other, seemingly unrelated, problems such as deposition and growth processes, or transport properties in random media [7]. In the case of fracture it has been established that crack surfaces scale as $W \sim L^\zeta$, where L is the system size, W is the roughness and ζ is the roughness exponent. Other scaling laws have been studied, e.g., in connection with the distribution of stresses, or for the total amount of damage found at various stages in the breakdown process.

By far the most popular tool in such studies has been the random fuse model [8]. In the fuse model, the nodes on the lattice are connected by current-carrying elements, i.e., fuses. The threshold for the amount of current which may flow through each fuse is chosen from a random distribution. Hence, in the breakdown process a fuse is irreversibly removed from the lattice once its threshold is exceeded. A new distribution of currents is then calculated before the next fuse is removed, and so on, until an uninterrupted path can be traced across the system. Although it really describes electrical breakdown, the fuse model is often referred to as a scalar model of fracture due to the similarity in form between Ohm's law and Hooke's law of linear elasticity. Results obtained for ζ with the fuse model are found to be different in two and three dimensions, however. The results are $\zeta = 0.74(2)$ in two dimensions [9] and $\zeta = 0.62(5)$ in three dimensions [10]. Although the former seems to agree with experimental find-

ings, the latter does not. Furthermore, the type of forces involved on the meso-scale also seem to make a difference, i.e., the results obtained with a scalar model differ from those obtained with a vectorial model. Specifically, in calculations with the elastic beam model $\zeta = 0.86(3)$ is obtained in two dimensions [11]. The difference between the results of the two and three dimensional fuse model indicates that the additional degrees of freedom afforded by the (three-dimensional) buckling beam model should provide a lower estimate for the roughness exponent in the vectorial problem as well. Since the observed value in real materials, i.e., $\zeta = 0.8$ [12], in fact does lie below the two dimensional beam lattice result, it would be interesting to see if the buckling beam lattice reproduces the universal value observed in nature.

However, although such fundamental aspects of the fracture process are certainly interesting, the subject of how buckling affects the scaling laws are left for future study. The focus in this paper is instead on the development of a lattice model that realistically includes the buckling behaviour observed in thin sheet materials. The characteristic out-of-plane deflection known as buckling is perhaps most frequently associated with thin plates or beams under compressive loading. Presently, however, we concern ourselves with the special case of a thin planar structure under tensile loading. The interaction of buckling with fracture in such circumstances is a well known phenomenon, although it has often been neglected in fracture mechanics analyses due to the extra complications involved. One of the characteristic features of buckling in a thin tension-loaded sheet is that a stable out-of-plane configuration is obtained after buckling has set in. This is in stark contrast with the case of compressive loading, where loss of stability usually signals complete breakdown.

Practically all previous work considers the effect buckling has on the strength properties of an already cracked plate or a plate with a geometrical discontinuity such as a circular hole or a rectangular cut-out. If the physical parameters of the plate are such that buckling can be expected before the crack begins to grow, the residual strength of the plate will be significantly lower than what would otherwise be expected, based on an analysis which does not take account of buckling. The present study of fracture and buckling will be more general in scope. In other words, we also regard sheets which, in their initial state, have no cracks or other discontinuities. Instead, cracks form by a complex process which depends on the evolving distribution of stresses and its interaction with a disordered meso-structure. The onset of buckling in this scenario, and the effect buckling has on the fracture properties, will vary according to the type of disorder used, i.e., weak or strong. Nonetheless, even for weak disorders the final crack which breaks the system will only rarely appear at the exact center of the sheet, and even then the situation will usually be complicated by additional cracks in the vicinity – cracks which interact with the main crack so as to alter the distribution of stresses and

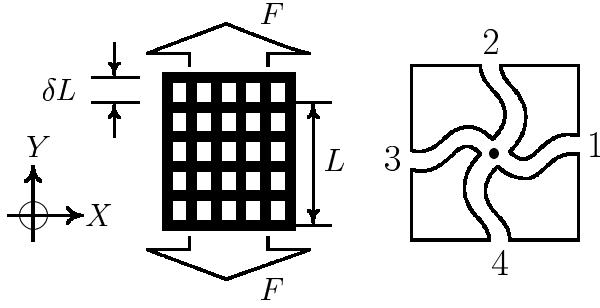


FIG. 1: On the left-hand side is shown a lattice of size $L = 5$ where a force couple has been applied uniformly on opposite edges. The strain imposed is consistent with mode-I type fracture and corresponds to a displacement $\delta L = 1$ in the Y -direction. The enumeration scheme of the neighbouring beams is shown on the right-hand side, where a rotation at node i (center dot) induces shearing forces and bending moments in the neighbouring beams.

hence also the exact shape or mode of buckling.

The emphasis here, however, is on the development of the model itself. For illustration purposes, a few results are included on uniform systems with a center-crack. In section II the plane beam model is briefly reviewed, before the equations describing the out-of-plane behaviour are derived in section III. Typical stress and displacement fields are shown in sections IV and V, respectively, before the initialization of buckling is discussed in section VI and a fracture criterion defined in section VII, where results for the buckling response ratio of a center-cracked sheet are included.

II. PLANE BEAM LATTICE

The beam model may be defined as a regular square lattice of size $L \times L$, where the spacing is one unit length, and each node in the horizontal and vertical in-plane directions is connected to its nearest neighbours by elastic beams. A beam is then fastened to other beams in such a way that, upon subsequent displacement of neighbouring nodes, the angle between beams remains the same as in the original underlying square lattice, see Fig. 1. Furthermore, all beams are imagined as having a certain thickness, providing finite shear elasticity.

Beginning with the simple two dimensional beam model, there are three possible degrees of freedom, i.e., translations in the horizontal (x) and vertical (y) directions, and rotations about the axis perpendicular to the plane (w). As shown in Fig. 1, this allows for both bending moments and transverse shearing forces, in addition to the axially tensile, or compressive, forces.

For any node i , the nearest neighbours j are numbered in an anti-clockwise manner, beginning with $j = 1$ to the right of i . Defining $\delta r = r_j - r_i$, where $r \in \{x, y, w\}$, the

forces on i due to $j = 1$ are

$${}_wM_i^{(1)} = \frac{1}{\beta + \frac{\gamma}{12}} \left[\frac{\beta}{\gamma} \delta w + \frac{\delta y}{2} - \frac{1}{3} (w_i + \frac{w_j}{2}) \right], \quad (1)$$

$${}_yT_i^{(1)} = \frac{1}{\beta + \frac{\gamma}{12}} \left[\delta y - \frac{1}{2} (w_i + w_j) \right], \quad (2)$$

$${}_xA_i^{(1)} = \frac{1}{\alpha} \delta x, \quad (3)$$

for the moment due to angular displacements w , shear and transverse force due to displacements y , and axial strain due to displacements x , respectively. Expressions for $j > 1$ are analogous.

Prefactors characteristic of the material and its dimensions are

$$\alpha = \frac{1}{E\rho}, \quad \beta = \frac{1}{G\rho}, \quad \gamma = \frac{1}{EI}, \quad (4)$$

where E is Young's modulus, ρ and I the area of the beam section and its moment of inertia about the centroidal axis, respectively, and G the shear modulus [13].

The conjugate gradient method [14] is used to obtain the displacement field from

$$\sum_j D_{ij} \begin{bmatrix} w_i \\ x_i \\ y_i \end{bmatrix} = \lambda \begin{bmatrix} W_i \\ X_i \\ Y_i \end{bmatrix}, \quad (5)$$

where

$$X_i = {}_xA_i^{(1)} + {}_xT_i^{(2)} + {}_xA_i^{(3)} + {}_xT_i^{(4)}, \quad (6)$$

$$Y_i = {}_yT_i^{(1)} + {}_yA_i^{(2)} + {}_yT_i^{(3)} + {}_yA_i^{(4)}, \quad (7)$$

$$W_i = \sum_{j=1}^4 {}_wM_i^{(j)}, \quad (8)$$

are the components of force and moment.

The material is assumed to be brittle, i.e., each beam is linearly elastic up to the breaking threshold. Using t_A and t_M for the thresholds in axial strain and bending moment, respectively, a good breaking criterion, inspired from Tresca's formula, is

$$\left(\frac{A}{t_A} \right)^2 + \frac{|M|}{t_M} \geq 1, \quad (9)$$

where $|M| = \max(|M_i|, |M_j|)$ is the largest of the moments at the two beam ends i and j .

The fracture process is initiated by imposing an external vertical displacement which at the top row corresponds to one beam-length, i.e., $\delta L = 1$, see Fig. 1. The lattice now consists of horizontally undeformed beams and beams which in the vertical direction are stretched lengthwise. The first beam to break is that for which the ratio A/t_A is largest, this being the vertically oriented beam which has the lowest value of t_A . If all threshold values are the same, the next beam to break will be one of the nearest lateral neighbours since these now

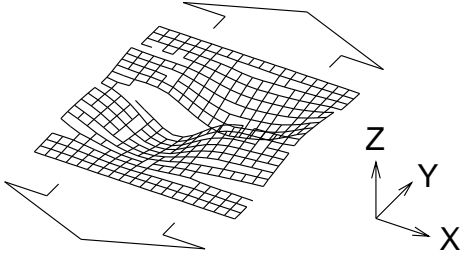


FIG. 2: A disordered beam lattice of size $L = 19$, which is strained to failure in mode-I type fracture, i.e., by applying a force couple at the top and bottom edges. The presence of a central crack leads to the build-up of compressive stresses around the crack edges, causing the structure to deflect out of the initial rest plane.

carry a larger load than other beams on the lattice. The case of no disorder is thus one in which the crack propagates horizontally from the initial damage, taking the shortest possible path to break the lattice apart. Introducing disorder in the breaking thresholds, material strength varies across the lattice and consequently the crack will not necessarily develop from the initial damage point. Instead microcracks and voids form wherever the stress concentration most exceeds the local strength, i.e., wherever Eq. (9) dictates that the next beam should be broken. Towards the end of the breakdown process smaller cracks merge into a macroscopic crack, forming a sinuous path which ultimately traverses the width of the lattice and thus breaks it apart, see, for instance, Fig. 2. In this scenario the quenched disorder on the thresholds and the non-uniform stress distribution combine to determine where the next break will occur. The stress distribution itself also continually changes as the damage spreads.

Throughout the process, the equilibrium stress field is re-calculated by use of Eq. (5) each time a beam is removed. The stress field therefore relaxes at a rate much faster than the process by which the crack grows. Hence, the model describes quasi-static fracture.

III. BUCKLING BEAM LATTICE

The displacements of a real material, even if its geometry is essentially confined to a plane, will generally occupy three dimensions. For instance, when opposite forces are applied uniformly along the top and bottom edges of a sheet of paper, with the object of straining it to failure, significant displacements will be observed in the direction perpendicular to the sheet, see Fig. 2. This becomes especially evident wherever sizable cracks appear. Reasons for this behaviour are deviations in the symmetry of the material itself, or its properties, about the plane through which the externally applied forces act. In some cases such deviations may simply correspond to an uneven thickness, or they may be caused by local variations in density, a gradient in the orientation of the micro

structure, and so forth.

To include this behaviour, the plane beam model must incorporate at least two additional features. One is the random variation of the material in the out-of-plane direction. Since lattice modeling reduces the material to a set of points corresponding to the nodes on a mathematically precise two-dimensional lattice, the most convenient approach is to impose a very small randomly chosen vertical displacement on each node. This is discussed in more detail in section VI. The other feature to be included, and the topic of the present section, is the physics of the forces which create, and maintain, the out-of-plane displacement field.

In the buckling beam model we have one translational and one rotational displacement relevant to each of the principal axes, i.e., six degrees of freedom, with the matrix system

$$\sum_j D_{ij} \begin{bmatrix} u_i \\ v_i \\ w_i \\ x_i \\ y_i \\ z_i \end{bmatrix} = \lambda \begin{bmatrix} U_i \\ V_i \\ W_i \\ X_i \\ Y_i \\ Z_i \end{bmatrix} \quad (10)$$

replacing Eq. (5). Presently the forces are projected onto the XY -, XZ and YZ -planes, and hence X_i of Eq. (10), that is,

$$X_i = \sum_{j=1}^4 X_i^{(j)}, \quad (11)$$

can be stated as

$$\begin{aligned} X_i = & \frac{A}{x} X X_i^{(1)} + \frac{T}{x} X Y_i^{(1)} + \frac{B}{x} X Y_i^{(1)} \\ & + \frac{T}{x} X Z_i^{(1)} + \frac{B}{x} X Z_i^{(1)} \\ & + \frac{A}{x} X Y_i^{(2)} + \frac{T}{x} X Y_i^{(2)} + \frac{B}{x} X Y_i^{(2)} \\ & + \frac{A}{x} X X_i^{(3)} + \frac{T}{x} X Y_i^{(3)} + \frac{B}{x} X Y_i^{(3)} \\ & + \frac{T}{x} X Z_i^{(3)} + \frac{B}{x} X Z_i^{(3)} \\ & + \frac{A}{x} X Y_i^{(4)} + \frac{T}{x} X Y_i^{(4)} + \frac{B}{x} X Y_i^{(4)}, \end{aligned} \quad (12)$$

where the term $\frac{B}{x} X Z_i^{(1)}$, for instance, is the x -component of the buckling (B) force due to $j = 1$, as projected onto the XZ -plane. Axial and transverse contributions are denoted (A) and (T), respectively.

The rotational displacements about the Y - and X -axes are denoted u and v , respectively, and z is used for vertical displacements along the Z -axis. A coordinate system is placed on each node, whereupon forces and moments are expressed as functions of the displacements. To this end, an elastic beam with no end restraints [15] is considered, as in the case of the plane model. In the buckling model, however, the coordinate system is additionally rotated about the relevant angle within the XZ -, YZ - or XY -plane, i.e., u , v or w .

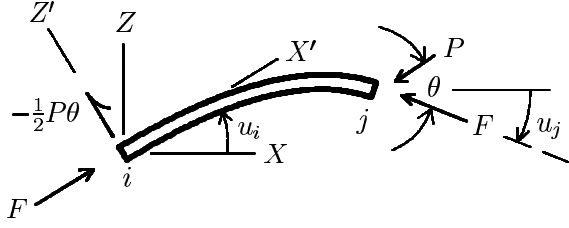


FIG. 3: The buckling term, $-\frac{1}{2}P\theta$, at node i due to $j = 1$ in the case of an axially compressive load, showing the angular displacements, u_i and u_j , the bending angle, θ , the axial force, F , and the component P , of F , which is parallel to the beam axis at node i . Also shown is the original XZ -system and the $X'Z'$ -system.

With the exception of the signs on the terms of

Eq. (12), contributions from neighbours $j = 1$ and $j = 3$ are similar, as are those from $j = 2$ and $j = 4$.

Consequently, if we define

$$p_j = \frac{1}{2}[1 - (-1)^j], \quad (13)$$

with $q_j = 1 - p_j$, and

$$r_j = \prod_{n=0}^{j-1} (-1)^n \quad (14)$$

with $s_j = (-1)^j r_j$, for notational convenience, then the total force on i along the X -axis, with the contributions from all four of the neighbouring beams having been included, reads

$$\begin{aligned} X_i = & \sum_{j=1}^4 F_i^{(j)} \left[p_j \cos w_i \cos u_i - q_j \sin w_i \cos v_i - \frac{\delta w}{2} \cos \delta w (p_j \sin w_i + q_j \cos w_i) \right. \\ & \left. - p_j \frac{\delta u}{2} \cos \delta u \sin u_i \right] s_j \\ & + \frac{1}{\beta + \frac{\gamma_Z}{12}} \sum_{j=1}^4 \left[(p_j \delta x + q_j \delta y) \sin w_i + (-1)^j (p_j \delta y + q_j \delta x) \cos w_i - s_j \left(\frac{\delta w}{2} + \sin w_i \right) \right] \\ & \times (p_j \sin w_i + q_j \cos w_i) \\ & + \frac{1}{\beta + \frac{\gamma_Y}{12}} \sum_{j=1}^4 \left[\delta x \sin u_i + (-1)^j \delta z \cos u_i + r_j \left(\frac{\delta u}{2} + \sin u_i \right) \right] p_j \sin u_i. \end{aligned} \quad (15)$$

In Eq. (15), moreover,

$$C(u, v) = p_j \frac{\delta u}{2} \left[\sin\left(\frac{\delta u}{2}\right) \right]^{-1} + q_j \frac{\delta v}{2} \left[\sin\left(\frac{\delta v}{2}\right) \right]^{-1} \quad (16)$$

is an angular correction to

$$F_i^{(j)} = \frac{1}{\alpha} \left\{ 1 - C(u, v) \sqrt{\delta z^2 + [1 - (p_j \delta x + q_j \delta y) s_j]^2} \right\}, \quad (17)$$

the latter being the projection onto the XZ -plane of the force along the axis of the beam. If we consider the $j = 1$ component in Eq. (12),

$${}^A_x X X_i^{(1)} = -F_i^{(1)} \cos w_i \cos u_i \quad (18)$$

is the contribution due to elongation or compression along the axis of the beam,

$${}^T_x X Y_i^{(1)} = \frac{1}{\beta + \frac{\gamma_Z}{12}} \left[(1 + \delta x) \sin w_i - \delta y \cos w_i + \frac{\delta w}{2} \right] \sin w_i \quad (19)$$

is due to forces which are transverse to the axis of the beam, and

$${}^B_x X Y_i^{(1)} = F_i^{(1)} \frac{\delta w}{2} \cos \delta w \sin w_i \quad (20)$$

is the contribution due to buckling. The latter arises when a beam in a bent configuration is under compressive or tensile axial loading, see, e.g., Fig. 3 where the term ${}^B_x X Z_i^{(1)}$ has been shown. Out-of-plane contributions with components along the X -axis are

$${}^T_x X Z_i^{(1)} = \frac{1}{\beta + \frac{\gamma_Y}{12}} \left[(1 + \delta x) \sin u_i - \delta z \cos u_i + \frac{\delta u}{2} \right] \sin u_i \quad (21)$$

from transverse forces, and

$${}^B_x X Z_i^{(1)} = F_i^{(1)} \frac{\delta u}{2} \cos \delta u \sin u_i \quad (22)$$

from buckling.

The buckling term, as obtained in the lowest order approximation, is essentially the product of a bending angle, θ , and an axial force component, P , the latter being parallel to the axis at the opposite end of the beam. The component of the buckling reaction in the $X'Z'$ -system which lies along the X -axis in the XZ -system is then ${}^B_x X Z_i^{(1)}$, i.e., Eq. (22).

Eq. (21), moreover, corresponds to that part of the transverse force (including shear) which does not include buckling and is similarly obtained, i.e., by rotating the axes in Eq. (2).

Finally, the axial term becomes

$$\lim_{u, z \rightarrow 0} {}^A_x X X_i^{(1)} = {}_x A_i^{(1)} \cos w_i \quad (23)$$

when the out-of-plane displacements are set to zero. Hence, in this case, only when the rotation of the XY -system onto the $X'Y'$ -system is neglected does Eq. (12) reduce to Eq. (3), of the plane beam model.

Although forces and displacements on a beam under simultaneous axial and transverse loading cannot, in general, be obtained by superposition, combinations such as ${}^T_x X Z_i^{(1)} + {}^B_x X Z_i^{(1)}$ in Eq. (12) result when only the leading terms, in P , are retained after inverting the expressions of Ref. [15]. This also causes the buckling term in tensile loading to be the same as that in compressive loading, a

change of sign being the only difference.

The expression for the Y -component is similar to that of the X -component, and is obtained by changing around the directions in Eq. (12), i.e.,

$$\begin{aligned} Y_i = & {}^A_y X Y_i^{(1)} + {}^T_y X Y_i^{(1)} + {}^B_y X Y_i^{(1)} \\ & + {}^A_y Y Y_i^{(2)} + {}^T_y X Y_i^{(2)} + {}^B_y X Y_i^{(2)} \\ & + {}^T_y Y Z_i^{(2)} + {}^B_y Y Z_i^{(2)} \\ & + {}^A_y X Y_i^{(3)} + {}^T_y X Y_i^{(3)} + {}^B_y X Y_i^{(3)} \\ & + {}^A_y Y Y_i^{(4)} + {}^T_y X Y_i^{(4)} + {}^B_y X Y_i^{(4)} \\ & + {}^T_y Y Z_i^{(4)} + {}^B_y Y Z_i^{(4)}. \end{aligned} \quad (24)$$

The Z -component, furthermore, is

$$\begin{aligned} Z_i = & {}^A_z X Z_i^{(1)} + {}^T_z X Z_i^{(1)} + {}^B_z X Z_i^{(1)} \\ & + {}^A_z Y Z_i^{(2)} + {}^T_z Y Z_i^{(2)} + {}^B_z Y Z_i^{(2)} \\ & + {}^A_z X Z_i^{(3)} + {}^T_z X Z_i^{(3)} + {}^B_z X Z_i^{(3)} \\ & + {}^A_z Y Z_i^{(4)} + {}^T_z Y Z_i^{(4)} + {}^B_z Y Z_i^{(4)}, \end{aligned} \quad (25)$$

i.e., also similar in form to Eq. (12) but with lines number two and five omitted.

The full expressions are then

$$\begin{aligned} Y_i = & \sum_{j=1}^4 F_i^{(j)} \left[q_j \cos w_i \cos v_i - p_j \sin w_i \cos u_i - \frac{\delta w}{2} \cos \delta w (p_j \cos w_i + q_j \sin w_i) \right. \\ & - \left. q_j \frac{\delta v}{2} \cos \delta v \sin v_i \right] r_j \\ & + \frac{1}{\beta + \frac{\gamma_Z}{12}} \sum_{j=1}^4 \left[(-1)^j (p_j \delta x + q_j \delta y) \sin w_i + (p_j \delta y + q_j \delta x) \cos w_i - r_j \left(\frac{\delta w}{2} + \sin w_i \right) \right] \\ & \times (p_j \cos w_i + q_j \sin w_i) \\ & + \frac{1}{\beta + \frac{\gamma_X}{12}} \sum_{j=1}^4 \left[(-1)^j \delta y \sin v_i - \delta z \cos v_i - s_j \left(\frac{\delta v}{2} + \sin v_i \right) \right] q_j \sin v_i \end{aligned} \quad (26)$$

for the force in the horizontal direction, and

$$\begin{aligned}
 Z_i = & - \sum_{j=1}^4 F_i^{(j)} \left(p_j \sin u_i - q_j \sin v_i + p_j \frac{\delta u}{2} \cos \delta u \cos u_i - q_j \frac{\delta v}{2} \cos \delta v \cos v_i \right) r_j, \\
 & - \frac{1}{\beta + \frac{\gamma_Y}{12}} \sum_{j=1}^4 \left[(1 + r_j \delta x) \sin u_i - r_j \delta z \cos u_i + \frac{\delta u}{2} \right] p_j \cos u_i \\
 & - \frac{1}{\beta + \frac{\gamma_X}{12}} \sum_{j=1}^4 \left[(1 - r_j \delta y) \sin v_i + r_j \delta z \cos v_i + \frac{\delta v}{2} \right] q_j \cos v_i
 \end{aligned} \tag{27}$$

for the force in the direction perpendicular to the rest plane.

Considering next the rotational contributions, a beam under axial loading, which is simultaneously bent, is shown in Fig. 4. In this case a buckling term arises which is again the product of a bending angle, θ , and an axial force component. For rotations about the Z-axis, this gives

$$W_i = {}^M_w X Y_i^{(1)} + {}^B_w X Y_i^{(1)} + {}^M_w X Y_i^{(2)} + {}^B_w X Y_i^{(2)} + {}^M_w X Y_i^{(3)} + {}^B_w X Y_i^{(3)} + {}^M_w X Y_i^{(4)} + {}^B_w X Y_i^{(4)}. \tag{28}$$

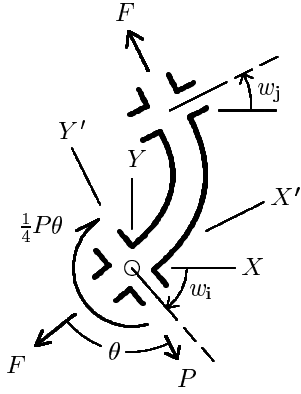


FIG. 4: The contribution $\frac{1}{4}P\theta$ to the in-plane moment at node i from $j = 2$, due to buckling, in the case of a tensile axial load. Shown are the angular displacements, w_i and w_j , the bending angle, θ , the axial force, F , and the component P , of F , which is parallel to the axis of the beam at the opposite end, i.e., at node $j = 2$.

For each beam in Eq. (28) there are two terms, one analogous to Eq. (1) and denoted (M), and one extra term, such as ${}^B_w X Y_i^{(1)}$, which is the contribution due to the beam being simultaneously bent while under axial loading. Similarly, we have

$$\begin{aligned}
 U_i = & {}^M_u X Z_i^{(1)} + {}^B_u X Z_i^{(1)} + {}^Q_u Y Y_i^{(2)} \\
 & + {}^M_u X Z_i^{(3)} + {}^B_u X Z_i^{(3)} + {}^Q_u Y Y_i^{(4)},
 \end{aligned} \tag{29}$$

for rotations about the Y-axis, and

$$\begin{aligned}
 V_i = & {}^Q_v X X_i^{(1)} + {}^M_v Y Z_i^{(2)} + {}^B_v Y Z_i^{(2)} \\
 & + {}^Q_v X X_i^{(3)} + {}^M_v Y Z_i^{(4)} + {}^B_v Y Z_i^{(4)},
 \end{aligned} \tag{30}$$

for rotations about the X-axis, where (Q) denotes the torque. In Eq. (29), the torque is simply

$${}^Q_u Y Y_i^{(2)} = \xi \delta u, \tag{31}$$

where, assuming $w > t$, the material constant is

$$\xi = G \frac{wt^3}{3} \tag{32}$$

when w denotes the width of the beam cross section and t its thickness. The buckling term reads

$${}^B_u X Z_i^{(1)} = -F_i^{(1)} \frac{\delta u}{4} \cos \delta u, \tag{33}$$

and that part of the bending moment which does not involve buckling becomes

$${}^M_u X Z_i^{(1)} = \frac{\beta}{\gamma_Y(\beta + \frac{\gamma_Y}{12})} \delta u - \frac{1}{2(\beta + \frac{\gamma_Y}{12})} \left[(1 + \delta u) \sin u_i - \delta z \cos u_i + \frac{\delta u}{3} \right] \tag{34}$$

when the axes are rotated. Eq. (29), when written out in full, is now

$$U_i = \frac{1}{\beta + \frac{\gamma_Y}{12}} \sum_{j=1}^4 p_j \left\{ \frac{\beta}{\gamma_Y} \delta u - \frac{1}{2} \left[(1 + r_j \delta x) \sin u_i - r_j \delta z \cos u_i + \frac{\delta u}{3} \right] \right\} - \sum_{j=1}^4 \left[F_i^{(j)} p_j \frac{\delta u}{4} \cos \delta u - q_j \xi \delta u \right] \tag{35}$$

and Eq. (30) is analogous, i.e.,

$$V_i = \frac{1}{\beta + \frac{\gamma_X}{12}} \sum_{j=1}^4 q_j \left\{ \frac{\beta}{\gamma_X} \delta v - \frac{1}{2} \left[(1 - r_j \delta y) \sin v_i + r_j \delta z \cos v_i + \frac{\delta v}{3} \right] \right\} - \sum_{j=1}^4 \left[F_i^{(j)} q_j \frac{\delta v}{4} \cos \delta v - p_j \xi \delta v \right]. \quad (36)$$

Finally, for rotations within the XY -plane, Eq. (28) becomes

$$W_i = -\frac{1}{2(\beta + \frac{\gamma_Z}{12})} \sum_{j=1}^4 \left[\sin w_i - s_j (p_j \delta x + q_j \delta y) \sin w_i - r_j (q_j \delta x + p_j \delta y) \cos w_i + \frac{\delta w}{3} \right] + \frac{\beta}{\gamma_Z(\beta + \frac{\gamma_Z}{12})} \sum_{j=1}^4 \delta w - \frac{1}{4} \sum_{j=1}^4 F_i^{(j)} \delta w \cos w_i. \quad (37)$$

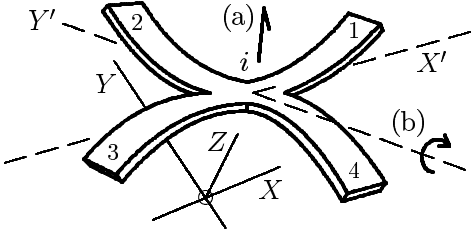


FIG. 5: Node i and its nearest neighbours $j = 1-4$, shown when the lattice is in an advanced state of buckling. The plane passing through i is uniquely defined by any j and $j \pm 1$ neighbours of i , as shown by the broken lines, and is no longer parallel to the XY -plane. The out-of-plane reaction (a) is normal to the $X'Y'$ -plane and (b) is a bending moment about the Y' -axis.

In the six components of Eq. (10), derived above, prefactors characteristic of the beam and its dimensions vary according to the principal axis of bending. Hence, in Eq. (4), we use

$$I_Z = \frac{1}{12} w^3 t \quad (38)$$

for bending within the XY -plane, and

$$I_X = \frac{1}{12} w t^3 = I_Y \quad (39)$$

for bending within the YZ - and XZ -planes. We have then assumed beams with a rectangular cross-section, as already noted in connection with Eq. (32). This is convenient in the study of how thin sheets behave during fracture, since one may then simply visualize beams with a flat profile, see Fig. 5. In the present calculations the chosen width-to-thickness ratio is 10:1, so that resistance towards bending within the plane is much larger than that which governs out of plane bending.

In the following, results are displayed for non-disordered systems with a central crack. To illustrate the nature of the forces, moments and displacements involved, sections of the lattice parallel with the crack are referred to as $J = 1, 2, \dots, L + 2$. Hence, on the bottom part of the lattice in Fig. 2, the set of nodes $i = 1$

to $i = L + 1$, located on the same row parallel with the X -axis, is referred to as $J = 1$. With a total of $L + 2$ rows J parallel with the Y -axis, the “near” edge of the crack coincides with $J = L/2 + 1$ while the “far” edge coincides with $J = L/2 + 1$. Likewise, the set of nodes $i = 1$ to $i = L + 2$ parallel with the Y -axis is referred to as, from left to right, $I = 1$ to $I = L + 1$.

IV. DISPLACEMENTS

The equations governing force and moment in a buckling beam lattice were derived in the previous section. At present we have not taken account of the Poisson contraction which is observed in elastic systems – at least not at the level of the individual beam. Such an effect does show up, however, on length scales spanning several beams. Of course, in the macroscopic behaviour of the lattice, an example of this is precisely the buckling behaviour we intend to study. The bulging of the crack edges shown in Fig. 2, for instance, comes about as a result of transverse compressive stresses which develop in the neighbourhood of the crack.

Fig. 6 shows the in-plane displacements x_i and y_i in a lattice of size $L = 100$ at various stages of crack advancement. The out-of-plane deflection $z_i(N)$ is also shown on the right-hand side. Displacements refer to the initial coordinate system on each node. In the specific example shown the crack grows towards the left-hand side of the lattice, with the out-of-plane deflection increasing with the extent of the crack opening. As previously mentioned, fracture is initialized by displacing the top row a unit distance. In the absence of geometrical discontinuities, each horizontal row J is then incrementally displaced by an amount $(L + 1)^{-1}$ with respect to the previous row $J - 1$. In the absence of cracks, the displacement field $y_i(J, N)$ then consists of a set of equidistant lines between zero and one. With a crack present, this is altered into the pattern shown in Fig. 6, e.g., for $y_i(0)$. As expected, transverse displacements $x_i(N)$ are largest close to the face of the crack. If we consider $x_i(0)$, and move from left to right along the edge of the crack,

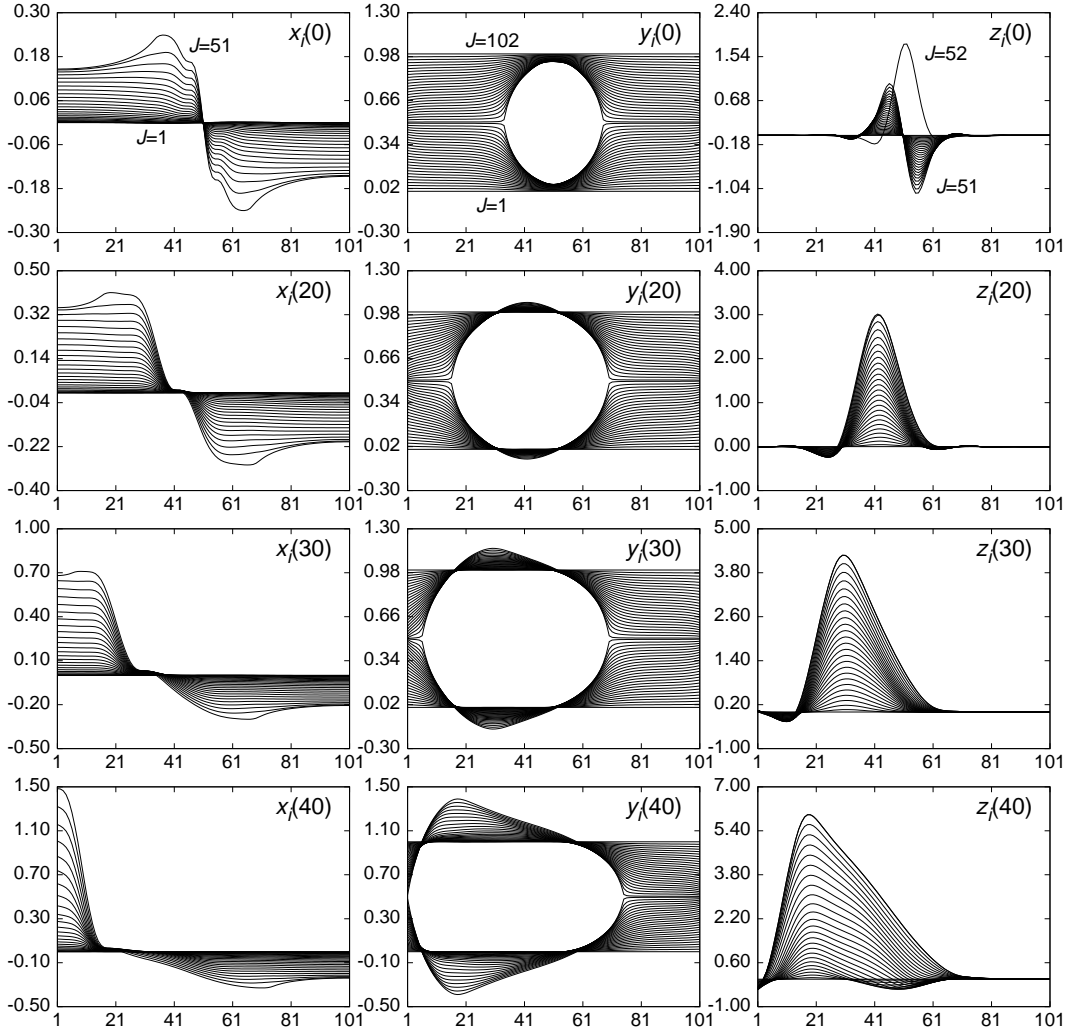


FIG. 6: Displacement fields across the width of a lattice of size $L = 100$ ($I = 1$ to $I = 101$) with an initial center-crack. On the left-hand side $x_i(N)$ is shown for $J = 1, 3, 5$, etc., up to and including the crack interface, i.e., $J = 51$. At center is shown $y_i(N)$ for $J = 1, 3, \dots, 102$. On the right-hand side, $z_i(N)$ is shown for $J = 1, 3, \dots, 51$, including also the far side of the crack interface, i.e., $J = 52$. The number of beams broken is N , and crack extent in the four stages shown is $I = 34 - 68$ ($N = 0$), $I = 16 - 70$ ($N = 20$), $I = 6 - 70$ ($N = 30$), and $I = 1 - 75$ ($N = 40$).

beams are seen to be stretched wherever the slope is positive and compressed wherever it is negative. As the crack grows the net effect, however, is to cause the lattice to contract in the transverse direction, e.g., with the edge on the left-hand side moving inward by about 1.5 beam lengths in the case of $x_i(40)$.

The rotation of axes mentioned above is necessary to obtain the correct feedback between the force components in the system, such as mutual consistency between XY -forces and the Z -forces. To illustrate this, regard the lattice before it begins to buckle, i.e., when the stress field is confined to the XY -plane. When a crack grows beyond a certain critical size, interaction between the stress field and random variations in the Z -direction initiates out-of-plane displacements which ultimately result in a buckled lattice. The driving forces are terms normal to the XY -plane, i.e., terms such as ${}^B_z X Z_i^{(1)}$ and ${}^B_z Y Z_i^{(2)}$,

which belong to $Z_i^{(1)}$ and $Z_i^{(2)}$, respectively. These terms are not large. In the flat lattice, for instance, the last two terms on the right-hand side of

$$X_i^{(1)} = {}^A_x X X_i^{(1)} + {}^T_x X Y_i^{(1)} + {}^B_x X Y_i^{(1)} + {}^T_x X Z_i^{(1)} + {}^B_x X Z_i^{(1)} \quad (40)$$

are identically zero while the terms ${}^T_x X Y_i^{(1)}$ and ${}^B_x X Y_i^{(1)}$ are very small in comparison with the leading axial term. The terms ${}^B_z X Z_i^{(1)}$ and ${}^B_z Y Z_i^{(2)}$, however, although being small in comparison with either ${}_x F_i^{(1)}$ or ${}_x T_i^{(2)}$, are non-negligible. This owes to the fact that there is no physical obstruction in the lattice to inhibit displacements in the Z -direction, i.e., there is no leading ${}_z Z Z_i$ term. Moreover, as can be seen from Fig. 5, when the lattice is in an advanced state of buckling there will be regions where the out-of-plane buckling reaction is inclined with

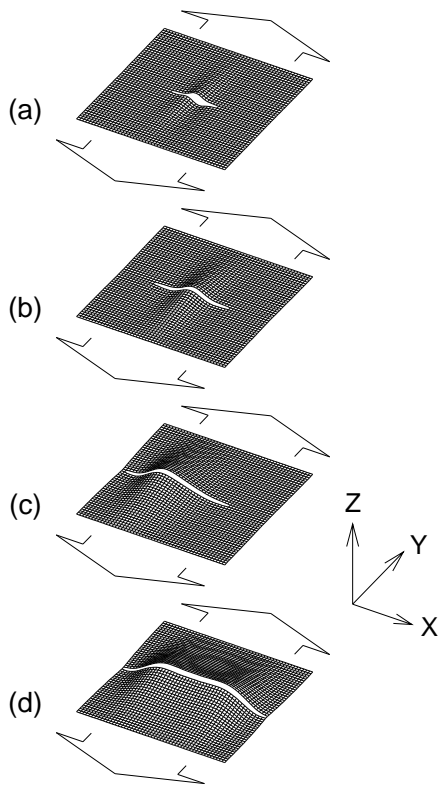


FIG. 7: A lattice of size $L = 50$, with an initial center-crack, shown at four different stages of fracture. The number beams broken are, from (a) to (d), $N = 0, 10, 20$, and 34 , respectively.

respect to the Z -axis, resulting in contributions of the type ${}^B_x X Z_i^{(1)} \neq 0$. These are smaller than ${}^B_z X Z_i^{(1)}$, but are also assumed to be non-negligible. In order to include such terms the axes are rotated to the local deflection of the lattice, whereupon the components along the X -, Y - and Z -axes are obtained.

An example of the effect this has is when a large crack, perpendicular to the force couple, opens up in the center of the lattice, as in Fig. 2 or Fig. 7. Although the initial displacement of the crack edges is normal to the rest plane, an in-plane component appears as the crack grows, i.e., the near edge of the crack is pulled slightly back along the negative Y -axis while the far edge is pulled forward in the opposite direction. This can be seen clearly in Fig. 6, where in $y_i(20)$ the rows nearest to the crack edges are displaced below or above the fixed values of the top and bottom rows. In the case of the near edge this means that displacements are negative, i.e., they have moved slightly backwards with respect to their equilibrium positions in the unrestrained-strained lattice. These displacements become more pronounced as the crack grows, as can be seen from $y_i(30)$ and $y_i(40)$.

It is particularly instructive to compare the displacements of a buckling lattice with those obtained for the same lattice when the out-of-plane degrees of freedom are

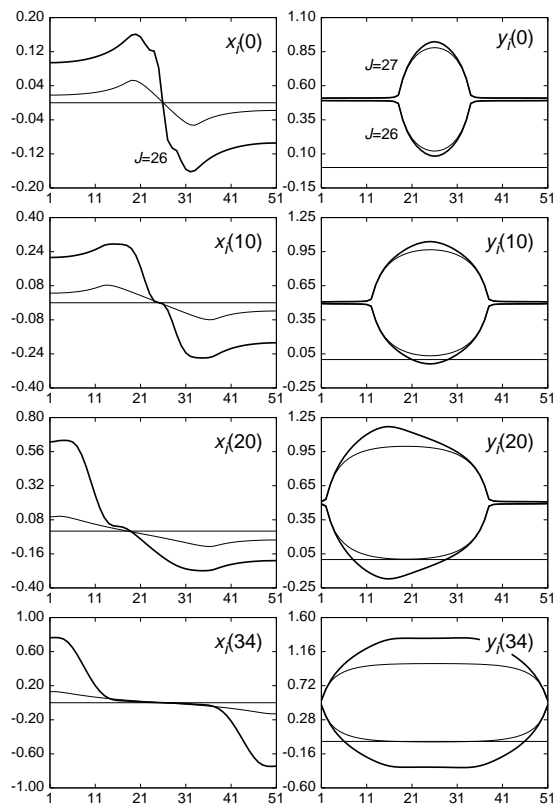


FIG. 8: Comparison between the crack-edge displacements, obtained for the buckling lattice shown in Fig. 7 (thick lines) and the same lattice when the out-of-plane degrees of freedom are suppressed (thin lines). At the top, the extent of the initial center-crack is $I = 18 - 34$. In subsequent stages, the crack extent is $I = 12 - 38$ ($N = 10$), $I = 2 - 38$ ($N = 20$) and $I = 1 - 51$ ($N = 34$). For $x_i(N)$ the near edge of the crack is shown and for $y_i(N)$ both edges are shown.

suppressed. In Fig. 7 a lattice of size $L = 50$ is shown in four stages of crack advancement. The corresponding in-plane displacements of the crack-edges are shown as thick lines in Fig. 8, with thin lines representing the same lattice in a non-buckling fracture mode. In the latter case, the y_i displacements are seen to be confined between the fixed values of the top and bottom row, the physical structure of the lattice itself effectively acting as an obstruction to displacements outside this range. A further feature that can be noted concerns the aforementioned ‘‘Poisson’’ contraction. This effect is seen to be present in a non-buckling lattice as well, although to a much lesser degree. As for the angular displacements w_i (not shown), these are seen to be somewhat larger in the buckling case, except for the peak values obtained at the crack tips, which are more or less the same. These peak values increase only as the crack nears the outer boundaries of the lattice, where x_i is large.

In general, the expressions derived for force and moment from Ref. [15] are accurate for small displacements only. This assumption we simply extend to all displacements. A second reason for rotating the axes, then, is

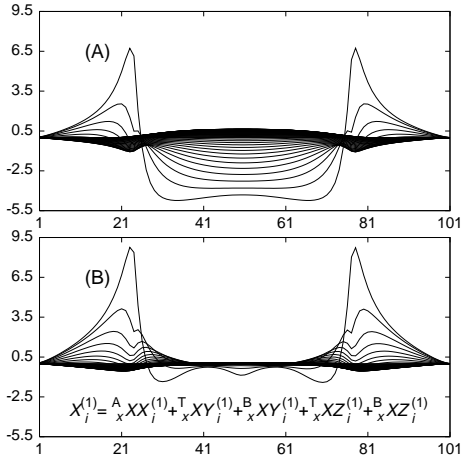


FIG. 9: Transverse stresses in a lattice of size $L = 100$ with a central crack which extends from $I = 24$ to $I = 78$. Shown are stresses in the non-buckling (A) and buckling (B) fracture modes, for every row J up to and including that which coincides with the near edge of the crack, i.e., $J = 51$. Negative values correspond to compressive stresses.

to conserve the consistency of the approximations used. To illustrate the point one may, for instance, regard a straight beam which, in its rest state, lies along the X -axis. The term ${}^T_z X Z_i^{(1)}$ then expresses the transverse force as a function of δz . When u_i is large, however, and the coordinate axes are fixed, δz , in addition to the transverse force, also implies some measure of axial strain in the beam even though this effect has already been included via Eq. (17). Hence, rotating the axes precludes the introduction of systematic errors, e.g., due to angular deflections of the lattice. It also improves the quality of the approximations used since angular displacements are rendered less severe in a rotated coordinate system. Large angular deflections usually involve a number of nodes on the lattice and hence by rotating the axes we avoid that too many errors accumulate.

It should also be pointed out, moreover, that with three rotational degrees of freedom there will in principle be several displacement combinations which correspond to a given space orientation of the beam axis. Hence the projection of forces into the XY - XZ - and YZ -planes is an approximation based on the assumption that large deflections about more than one axis simultaneously are rare. Otherwise the exact orientation of the beam would be history-dependent, i.e., it would depend on the sequence in which the (final) angular displacements u_i , v_i and w_i were incremented.

V. FORCE COMPONENTS

The out-of-plane force components are small, but their collective effect has a significant impact on the stress field. In the presence of significant cracks there is a feedback from the Z -displacements which allows the XY -

displacements of the buckled lattice to relax with respect to the XY -displacements of the flat lattice. One example of this is the transverse compressive stress stored in the region in front of and behind the crack in the non-buckling lattice. Buckling releases this stress, as can be seen in Fig. 9, where the $j = 1$ component of Eq. (11) is shown in the non-buckling (A) and the buckling (B) cases. In (A) a region of compressive stress confined between the crack tips is seen to extend for a distance of about 6-8 rows away from the crack edge. In (B) only a vestige of this is left, and then only in the immediate vicinity of the crack. The tensile stress at the crack tips increases slightly in the buckled configuration.

In the non-buckling beam model, the extra non-linear terms which arise when the beam is simultaneously bent while under axial compression, or tension, are of lesser importance. All forces now act within the structure which defines the plane so that, in calculating the in-plane displacement field, corrections such as those due to w_i in Eq. (23) may be neglected. The out-of-plane displacement field, on the other hand, is obtained from an equilibrium state in force and moment between a number of terms which are individually small.

For instance, the axial, transverse and buckling components which make up the $j = 1$ contribution to Eq. (25) are shown in Fig. 10. Here the vertical scales on the three subplots have been adjusted to the relative sizes of the components. The magnitudes, furthermore, refer to the scale of Fig. 9 and thus gives an idea of the “smallness” of the out-of-plane force components. In agreement with Fig. 9, the forces in Fig. 10 are seen to be most significant within a region nearest to the crack edge, extending about 6-8 rows to either side of the crack. At the onset of buckling the axial and transverse terms, ${}^A_z X Z_i^{(1)}$ and ${}^T_z X Z_i^{(1)}$, are identically zero while the buckling term, ${}^B_z X Z_i^{(1)}$ shown in Fig. 3, is non-zero. In this-situation the sum of contributions from $j = 1 - 4$ is non-zero. As the out-of-plane deflection increases, an equilibrium is approached where the sum of forces is zero. At this equilibrium the buckling terms, e.g., terms such as ${}^B_z X Z_i^{(1)}$ in Fig. 10, remain non-zero. This is also the case with the out-of-plane moments, shown in Fig. 11. The three subplots are not mutually to scale in this case, but the magnitudes again refer to the scale of Fig. 9. Out-of-plane moments are seen to be somewhat larger than the axial and transverse buckling forces of Fig. 10. Hence, at the equilibrium, the most significant of the non-linear terms are those relevant to the momentum, ${}^B_u X Z_i^{(1)}$ being about five times larger than ${}^B_z X Z_i^{(1)}$.

It is instructive to see what happens when buckling terms such as ${}^B_z X Z_i^{(1)}$ and ${}^B_u X Z_i^{(1)}$ are removed. Shown in Fig. 12, at the onset of buckling, is the movement of the crack-edge as a function of time, the time-steps being defined by the iteration procedure which locates the equilibrium of force and moment. Just before the point at which equilibrium is reached, all buckling terms are “switched off” whereupon the remaining forces set about

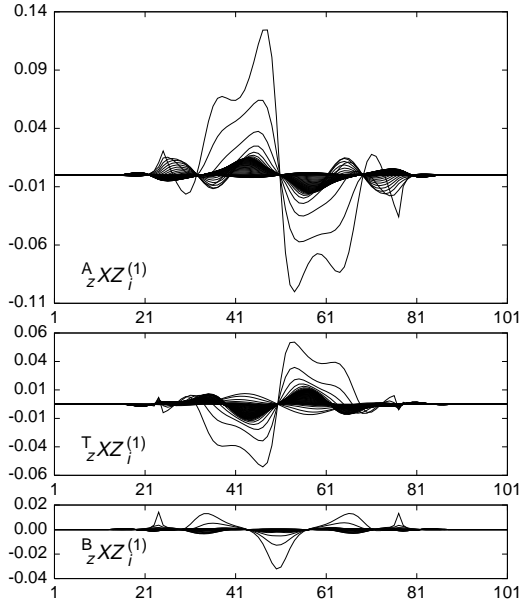


FIG. 10: Out-of-plane force components. Shown are the axial $A_z X Z_i^{(1)}$, transverse $T_z X Z_i^{(1)}$, and buckling $B_z X Z_i^{(1)}$ contributions to $Z_i^{(1)}$ of Eq. (25). Contributions to $Z_i^{(3)}$ are similar, but with the contours of $A_z X Z_i^{(3)}$ and $T_z X Z_i^{(3)}$ being mirror reflections of $A_z X Z_i^{(1)}$ and $T_z X Z_i^{(1)}$ about $I = 51$. Contributions to $Z_i^{(2)}$ and $Z_i^{(4)}$ are smaller. Lattice parameters used and contours shown are the same as in Fig. 9.

to locate a new minimum of elastic energy. This new minimum, of course, is none other than the flat configuration. As would be expected, not only do terms such as $B_z X Z_i^{(1)}$ and $B_u X Z_i^{(1)}$ cause buckling, they also sustain it once it has been established.

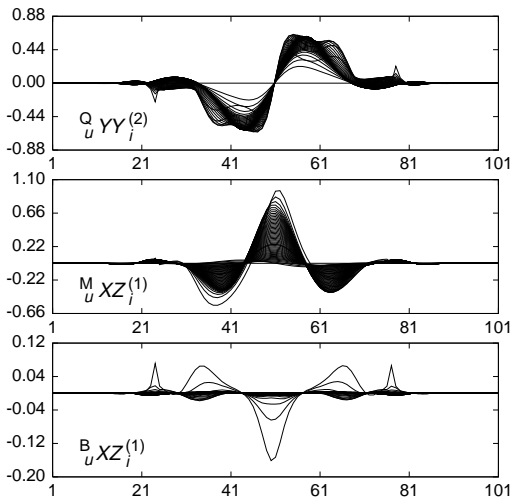


FIG. 11: Out-of-plane moment components about the Y-axis. Shown are the torsional $Q_u Y Y_i^{(2)}$, axial $M_u X Z_i^{(1)}$, and buckling $B_u X Z_i^{(1)}$ contributions to U_i in Eq. (29). Lattice parameters used and contours shown are the same as in Fig. 9.

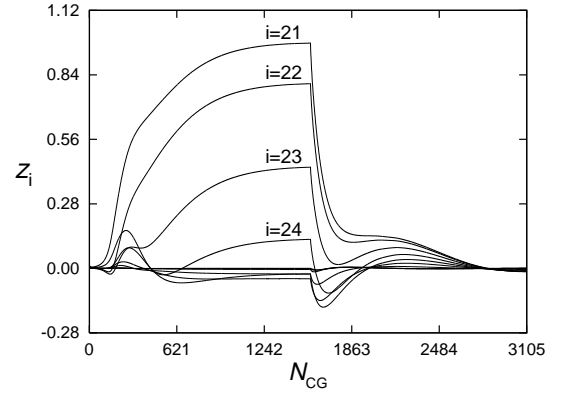


FIG. 12: The movement of the crack-edge as a function of the time-steps in the numerical iteration, shown for a lattice of size $L = 40$ at the onset of buckling and for a central crack between $I = 14$ and $I = 28$. Just prior to the point at which the equilibrium is reached, at time $T_{CG} = 1570$, all terms such as $B_z X Z_i^{(1)}$ are “switched off”.

Finally some remarks on the angular correction in Eq. (17), which is included to allow for the possibility that axial force may increase or decrease as a consequence of bending. In Eq. (17) it is assumed that the additional elongation due to bending can be obtained from a multiplicative factor. This factor is based on the ratio of a circular arc [16] to a straight line, the former being the semi-circle defined by the angular difference δu at the end-points and the latter the line which connects these. On the level of the individual beam, the presence of inflection points are neglected in this approximation. In other words, up-down curvatures may only occur in combinations of two or more beams in an end-to-end alignment. Furthermore, as can be seen from Eq. (17), the effect of in-plane bending moments, or transverse displacements perpendicular to the rest axis of the beam, are neglected as contributions which would otherwise add to the axial length of a beam.

VI. INITIALIZING THE OUT-OF-PLANE DEFLECTION

An important feature to be included in the model is the random variation of the material in the out-of-plane direction, as was remarked in section III. In thin materials such as paper, cloth, membranes and so forth, the most important factor influencing the behaviour during fracture is not the three-dimensional structure of the material itself. Rather it is the out-of-plane deflection of this structure which makes a difference. Nevertheless, random variations in the thickness direction provide an important part of the mechanism which initiates buckling. This is because such variations combine with the externally applied force and the emerging cracks to create local forces and moments which are not perfectly aligned within the plane. Once a buckled configuration has been

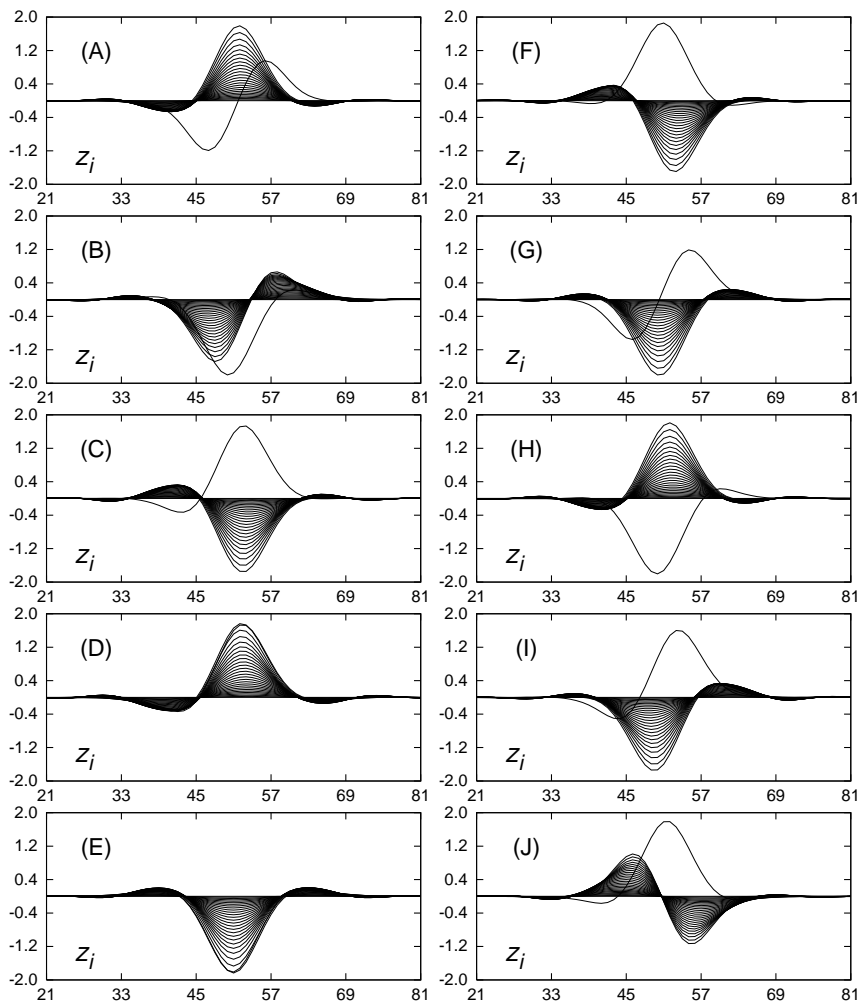


FIG. 13: Buckling modes for ten samples of a lattice of size $L = 100$, with a center-crack between $I = 34$ and $I = 68$. For the lower half of the lattice, contours of every other row $J = 1, 3, \dots$, are shown, up to and including $J = 51$, i.e., the near edge of the crack. The far edge, $J = 52$, is also shown. The only difference between the samples is the random variation used to initialize the out-of-plane deflection.

established, however, the variation in the thickness direction is far less important.

Since we presently regard the out-of-plane deflection of a structure which has no vertical extent, buckling must be initiated by other means. Specifically, in modeling the fracture process, the equilibrium stress field is recalculated by use of Eq. (10) after a beam has been removed. At each step of this process, i.e., for each beam removed, a sample-specific random noise in the form of a small vertical displacement is imposed on all nodes of the lattice. Presently, we use a random number uniformly distributed on the interval $[-0.01, 0.01]$. In the early stages of the fracture process, the stress field is calculated in the presence of these variations until buckling commences. Before sizable cracks appear, forces combine to flatten out the vertical displacements. That is, a flat configuration is energetically preferred to begin with, and fracture propagates according to the non-buckling simulation. As significant cracks begin to appear, however,

the conditions at some point become favourable for the out-of-plane components of the stress field to be realized, and buckling sets in. From here on the random noise is discarded, and the next displacement configuration is simply calculated from the previous coordinates. When the lattice has been broken, a new set of vertical displacements is generated for the next sample, i.e., a sample-specific random noise is used.

Lattice buckling modes in the presence of a center-crack of size $\sim L/3$ are shown in Fig. 13. The only disorder present here is that due to the out-of-plane initialization, but evidently a number of buckling modes may appear. In the following, cases where the deflection of the edges of the crack is to the same side, i.e., up-up or down-down, are referred to as symmetric buckling, and cases where the deflection is to opposite sides is referred to as anti-symmetric buckling. In Fig. 13, (D) and (E) are examples of the former, and (F) and (H) are examples of the latter. Another buckling mode which frequently ap-

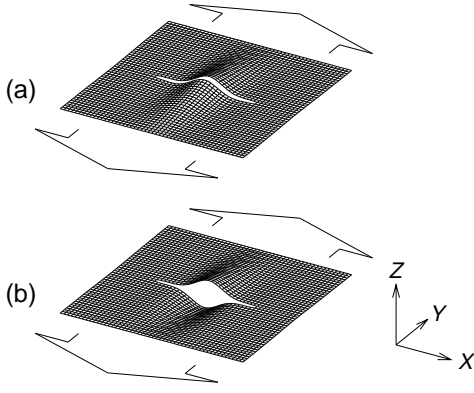


FIG. 14: A beam lattice of size $L = 50$, showing (a) the symmetric and (b) the anti-symmetric buckling modes for a crack between $I = 12$ and $I = 40$.

pears is that shown in (A), (G) or (J), where the main bulge at one of the crack edges is made up of four, rather than three, half-waves. Based on the few dozen samples observed, (A) and (J) evolve into type (D) after a few more beams have been broken, and (G) into type (E), i.e., the symmetric buckling mode prevails in each case. However, due to the randomness introduced, examples such as (H) are not completely anti-symmetric about the neutral plane. Hence, even for this simple crack configuration, the exact shape of the out-of-plane deflection can vary considerably. The overall shape, however, tends to fall within the main categories, i.e., one of the two symmetric or anti-symmetric buckling modes. This way of initializing the out-of-plane deflection is suitable for studying disordered systems, where a lattice without any initial geometrical discontinuity is strained until random cracks begin to appear. As the cracks grow buckling sets in at some point, depending on the configuration, position and size of the initial cracks.

Another way of initializing the out-of-plane deflection is to impose a small vertical deflection on a very few nodes in strategic positions. This is most practical when studying an “ideal” buckling scenario, such as the fracture of a non-disordered plate with a perfect center-crack.

VII. FRACTURE CRITERION

In order to study how buckling affects the fracture properties of a two-dimensional structure an appropriate breaking criterion should be chosen. As previously mentioned, this can be done to suit a range of engineering requirements. Often the mode of rupture in the out-of-plane direction is radically different from that which takes place within the plane. In paper or cloth, for instance, the phenomenon which first springs to mind is tearing. The energy required to propagate a crack across a given area in tear mode is much less than that which causes the same area to fracture in pure tensile loading. This is especially the case with paper.

Out-of-plane contributions to the breaking criterion must be included by some other mechanism than that provided by Eq. (9), since the latter is relevant to regions which are comparable in size to a beam. The stress intensification due to buckling, on the other hand, is due to much smaller regions, i.e., comparable in extent to the sharp crack tip. One way of enhancing the stress due to buckling is to combine torsion with axial stress. The larger the load, the more sensitive the beam will be to the presence of a given amount of torque. Compressive loads are assumed to alleviate the torsional moment, but only to a very small degree.

Hence, the breaking criterion can be stated as

$$\left(\frac{F_C}{t_{F_C}}\right)^2 + \frac{|\mu_C|}{t_{\mu_C}} \geq 1, \quad (41)$$

where

$$F_C = F_i^{(j)} - \chi |Q_i^{(j)}| \quad (42)$$

is the effective stress,

$$Q_i^{(j)} = p_j \cdot {}^Q_v X X_i^{(j)} + q_j \cdot {}^Q_u Y Y_i^{(j)} \quad (43)$$

the torque, and μ_C the combined bending moment. With w and t denoting the width and thickness, respectively, of the beam,

$$\sigma = \frac{w}{t} \quad (44)$$

is the aspect ratio of the cross section, and

$$\chi = \begin{cases} 1 + \sigma^2 L |F_i^{(j)}| L_0, & F_i^{(j)} < 0, \\ 1, & F_i^{(j)} \geq 0, \end{cases} \quad (45)$$

is the enhancement factor in Eq. (42).

Considering Fig. 14, the breaking stress is increased in case (b) and also in case (a) provided the deflections in front of and behind the crack are not congruent. When the bulges are completely symmetric, however, (a) does not intensify the breaking stress and thus contradicts experimental findings.

Another possibility is to assume a crack-tip stress enhancement which depends on the out-of-plane bending moment. Here the in-plane displacement component y_i observed in Fig. 8, i.e., the backward and forward movement of the crack edge, creates an angular displacement about the X -axis. For a sufficiently thin plate the resistance towards bending will not be sufficient to halt the out-of-plane deflection once it has commenced, since the forces involved act over a region much larger than the immediate neighbourhood of the crack. Due to the short distance which separates the top and bottom surfaces, the resulting “lever-arm” effect creates an asymmetric stress-gradient across the crack front in the direction of the thickness. Whereas tensile force on the concave side is then reduced, it increases on the convex side. This

increase comes in addition to the stress already concentrated along the crack front, i.e., the very presence of a crack creates a screening effect which re-distributes the in-plane stresses so as to cause a build-up in the load at the crack tips. For a crack that has grown to an extent which allows buckling to occur, this in-plane stress is significant. The crack-tip opening angle also plays an important role. Buckling in brittle materials, for instance, is known to have a profound effect on the maximum load the system can tolerate before breaking. In a FEM study by Seshadri and Newman [17] a hypothetical very large critical crack-tip opening angle was used to model buckling in a ductile material. Strength reduction in this case was found to be significantly smaller than for brittle materials.

In the beam model, the crack tip is never sharper than exactly one beam length. To emulate the above stress enhancement due to out-of-plane bending we instead imagine a sharp crack to be embedded within that beam which on the lattice defines the tip of the crack, and consider a combination of axial stress and moment. Out-of-plane bending modes are shown in Figs. 15 and 16, where the displacements of the schematic lattice at the top have been exaggerated somewhat to illustrate the point. Specifically, the Z -displacements of contour B have been scaled up 100 times with respect to those of contour A, which itself is scaled up with respect to the horizontal extent of the lattice. The in-plane Y -displacements have also been adjusted accordingly.

Experimental evidence indicates that the stress enhancement at the crack tips is more or less similar in the symmetric and anti-symmetric buckling modes. To incorporate this we distinguish between the two cases. Hence, retaining Eq. (41), we introduce

$$\widetilde{M}_i^{(j)} = \frac{M_i^{(j)}}{|M_i^{(j)}|}, \quad (46)$$

where

$$M_i^{(j)} = p_j \left({}^M_u X Z_i^{(j)} + {}^B_u X Z_i^{(j)} \right) + q_j \left({}^M_v Y Z_i^{(j)} + {}^B_v Y Z_i^{(j)} \right) \quad (47)$$

replaces $Q_i^{(j)}$ in Eq. (42). In this prescription,

$$\widetilde{M}_i^{(j)} = \pm \widetilde{M}_j^{(i)} \quad (48)$$

denotes symmetric (−) or anti-symmetric (+) buckling, respectively, with the signs referring to the direction of the moment at the two beam ends.

For the effective stress in the beam, we now use

$$F_C = F_i^{(j)} - \widehat{\chi} |M_i^{(j)} - M_j^{(i)}| \quad (49)$$

in the symmetric case, i.e., when

$$\widetilde{M}_i^{(j)} = -\widetilde{M}_j^{(i)}, \quad (50)$$

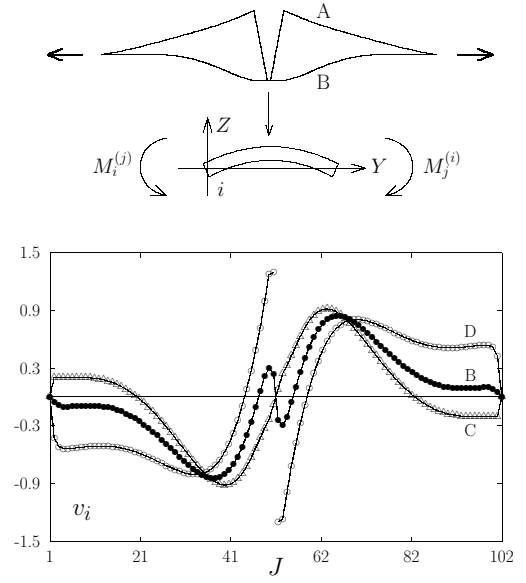


FIG. 15: Symmetric buckling. Shown at top, for a lattice of size $L = 100$, is (A) the $I = 51$ contour, passing through the middle of the lattice, and (B) the $I = 34$ contour, passing through the left-hand side crack tip. Also shown is the bending mode of the beam which defines the crack tip at the junction between $I = 34$ and $J = 51$. At the bottom are shown the out-of-plane angular displacements v_i about the X -axis, in the case of (B) above. Also shown are the neighbouring contours, (C) $I = 33$ and (D) $I = 35$, where (D) is discontinuous due to the intersecting crack.

and

$$F_C = F_i^{(j)} - \frac{1}{2} \widehat{\chi} \max(|M_i^{(j)}|, |M_j^{(i)}|) \quad (51)$$

in the anti-symmetric case, i.e., when

$$\widetilde{M}_i^{(j)} = \widetilde{M}_j^{(i)}. \quad (52)$$

The enhancement factor in Eqs. (49) and (51) is

$$\widehat{\chi} = \begin{cases} \widehat{\Lambda}_i (1 + \sigma^2 L |F_i^{(j)}| L_0), & F_i^{(j)} < 0, \\ 0, & F_i^{(j)} \geq 0, \end{cases} \quad (53)$$

where

$$\widehat{\Lambda}_i = p_i \widehat{\Lambda}_{i,x} + q_i \widehat{\Lambda}_{i,y} \quad (54)$$

is a discontinuity operator. The choice made above causes the breaking stress of the beams at the crack tips to increase by a comparable amount in symmetric and anti-symmetric buckling.

The expressions for χ and $\widehat{\chi}$ in Eqs. (45) and (53), respectively, have been chosen, very generally, to incorporate some overall effects related to size, material and relative dimensions. Hence, it is reasonable to assume that, for a given size, “tearability”, or the “lever-arm” effect, increases with decreasing sheet, or plate, thickness. In conjunction with this, the crack-tip opening an-

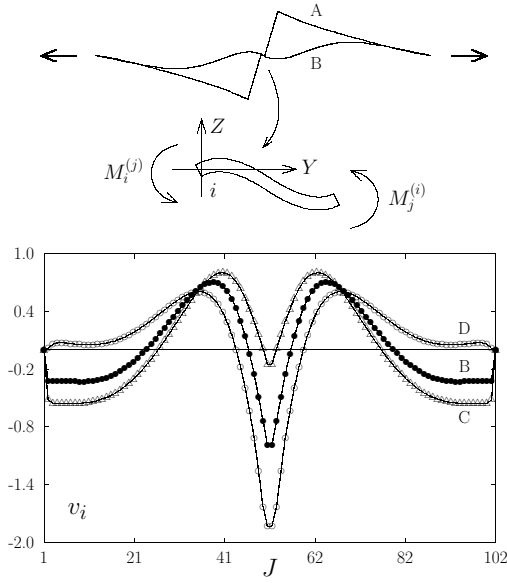


FIG. 16: Anti-symmetric buckling. Shown at top, for a lattice of size $L = 100$, is (A) the $I = 51$ contour, passing through the middle of the lattice, and (B) the $I = 34$ contour, passing through the left-hand side crack tip. Also shown schematically is the beam which defines the crack tip at the junction between $I = 34$ and $J = 51$. Although the bending mode is correct, the actual angles at the ends of the beam are negative and not positive as shown. Out-of-plane angular displacements v_i about the X -axis are included at the bottom, with the notation being the same as in Fig. 15.

gle, which decreases with increasing resistance towards in-plane bending, also enters the picture. Both effects are presently included via the ratio of the in-plane to the out-of-plane inertial moment for bending, i.e., $\sigma^2 = I_Z/I_X$. The length of the arm with which the out-of-plane forces act is assumed to be proportional to the vertical extent of the buckling zone. Since this, in turn, is proportional to system size, a factor $L|F_i^{(j)}|$ is also included. As noted previously, fracture is initiated by displacing the top row of the lattice a fixed distance, usually corresponding to one beam length. To avoid scale effects associated with this, a further factor L_0 is included, where L_0 is the size of the reference system for which the top row displacement is exactly one beam length. The introduction of a reference system allows for the possibility of comparing systems of varying size where the physical behaviour involved requires the same relative external boundary conditions. For instance, referring to the intact lattice, mode-I loading then imposes the same initial strain of $(L_0 + 1)^{-1}$ on each beam. Although computational time increases when $L > L_0$, features such as how various buckling modes appear with respect to system size will depend on the external loading. Otherwise, $L_0 = L$ might probably be used in cases where we are interested in features which depend on the internal processes of the fracture mechanism, such as the roughness exponent of crack interfaces.

To guard against unphysical breaks, we introduce

$$\hat{P}_{y,i} = n_{y,i-1} + n_{y,i+1} \quad (55)$$

which contributes when one or both nearest lateral neighbours are intact, and

$$\hat{Q}_{y,i} = \prod_{j=1}^{C_{L,m}-1} (1 - n_{y,i-j}) + \prod_{j=1}^{C_{L,m}-1} (1 - n_{y,i+j}) \quad (56)$$

which contributes when a certain number of neighbours have been broken. For any node i , the array

$$n_{y,i} = \begin{cases} 0 \\ 1 \end{cases} \quad (57)$$

now keeps track of the status of the beam which extends away from i in the direction of the Y -axis, i.e., it remembers whether this is broken or intact, respectively. The combined expression,

$$\hat{\Lambda}_{y,i} = \hat{P}_{y,i} \cdot \hat{Q}_{y,i}, \quad (58)$$

has the property

$$\hat{\Lambda}_{y,i} = \begin{cases} 0 \\ 1 \end{cases} \quad (59)$$

as has $\Lambda_{x,i}$ governing cracks in the normal direction. In other words, Eq. (54) ensures that the stress enhancement mechanism is activated only in cases where the lateral neighbour on one side is intact while simultaneously a certain number of beams, defining a minimum crack length $C_{L,m}$, are broken on the other side.

In most cases the operator Λ_i is not necessary. It has been included to avoid cracking being induced near the top and bottom rows of the lattice. For very large systems, and especially in cases where L is significantly larger than L_0 , breaks sometimes occur due to the large angular gradients in beams extending up from $J = 1$ or down from $J = L+2$, see, for instance, Figs. 15 and 16. In the present formalism the properties of beams with inflection points are not considered, the smallest crack that can cause buckling, i.e., a bulge consisting of at least three half-waves, is therefore approximately $C_{L,m} = 4$. This is confirmed in numerical runs for systems with small L , but where $L \gg L_0$. A problem with using such a large value of $C_{L,m}$ is that it excludes cracks inclined at an angle with respect to the horizontal. Over a wide range of system parameters and external boundary conditions, however, $C_{L,m} = 2$ was found to be adequate.

In the limit of no buckling, i.e., $\delta v \rightarrow 0$ or $\delta u \rightarrow 0$, Eq. (41) reduces to Eq. (9). In other words, if buckling is not activated, then neither is the stress enhancement mechanism in the fracture criterion.

Finally, in order to illustrate how Eq. (41), with Eqs. (46) to (59) defining the stress enhancement mechanism, works within our model of buckling, we consider the buckling response ratio of the residual strength of the

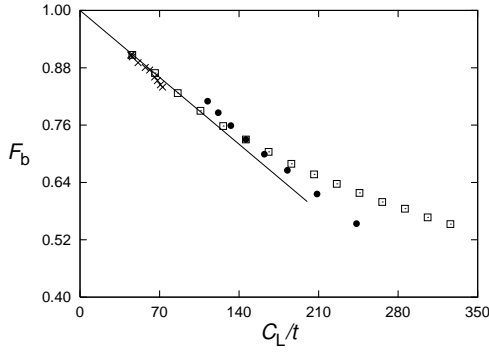


FIG. 17: The buckling response ratio, F_b , shown as a function of the crack-length-to-thickness ratio, C_L/t , for various systems with $L = 3C_L$. Open squares denote the results of varying L while keeping t constant, filled circles denote the results of varying t with $L = 54$ fixed, and crosses denote similar results with $L = 24$ fixed. Kuhn and Figge's linear expression [18] is also included for comparison.

system. That is, $F_b = \lambda_0/\lambda_z$, where λ_0 and λ_z represent the maximum applied external force a restrained or buckled plate, respectively, can tolerate before breaking apart. Early experimental results show that the decrease in strength due to buckling increases as the ratio of the

crack-length C_L to the thickness t is increased. A linear relationship was proposed by Kuhn and Figge [18] which, in the case of brittle materials, has been shown to agree well with more recent FEM calculations [17]. In Fig. 17, results obtained with the beam model are compared with the Kuhn-Figge relationship. A small correction to the size of the central crack has been made to account for the finite size of the beams. The effect is very small, shifting the values of the smallest systems slightly to the left, thus improving the agreement with the Kuhn-Figge relationship from very good to excellent.

VIII. SUMMARY

To summarize, we have included the additional degrees of freedom necessary to describe the interaction of cracks with buckling in the elastic beam model. This model is stochastic in nature, so that sheets with random cracking at any level of meso-structural disorder can be studied, including systems with no disorder. In addition to important issues of practical relevance in traditional fracture mechanics, such as strength properties and stability, the present model also enables fundamental aspects of fracture in random media to be explored.

-
- [1] See, e.g., H. J. Herrmann and S. Roux, *Statistical Models for the Fracture of Disordered Media*, (North-Holland, Amsterdam, 1990).
 - [2] S. Roux and E. Guyon, J. Phys. (Paris) Lett. **46**, L999 (1985).
 - [3] R. G. Forman, "Experimental Program to Determine Effect of Crack Buckling and Specimen Dimensions on Fracture Toughness of Thin Sheet Materials", Technical Report AFFDL-TR-65-146, Air Force Flight Dynamics Laboratory, Dayton, Ohio (1966).
 - [4] J. R. Dixon and J. S. Strannigan, "Stress Distributions and Buckling in Thin Sheets with Central Slits", in *Proc. Second Int. Conf. on Fracture*, pp. 105-118, edited by P. L. Pratt *et al.*, (Chapman and Hall, 1969).
 - [5] G. F. Zielsdorff and R. L. Carlson, Eng. Fract. Mech. **4**, 939 (1972).
 - [6] B. B. Mandelbrot, D. E. Passoja and A. J. Paullay, Nature **308**, 721 (1984).
 - [7] A. L. Barabasi and H. E. Stanley, *Fractal Concept in Surface Growth*, (Cambridge University Press, Cambridge, England, 1995).
 - [8] L. de Arcangelis, S. Redner and H. J. Herrmann, J. Phys. (Paris) Lett. **46**, L585 (1985).
 - [9] A. Hansen, E. L. Hinrichsen and S. Roux, Phys. Rev. Lett. **66**, 2476 (1991).
 - [10] G. G. Batrouni and A. Hansen, Phys. Rev. Lett. **80**, 325 (1998).
 - [11] B. Skjetne, T. Helle and A. Hansen, Phys. Rev. Lett. **87**, 125503 (2001).
 - [12] E. Bouchaud, J. Phys. Condens. Matter **9**, 4319 (1997).
 - [13] H. J. Herrmann, A. Hansen and S. Roux, Phys. Rev. B **39**, 637 (1989).
 - [14] M. R. Hestenes and E. Stiefel, Nat. Bur. Stand. J. Res. **49**, 409 (1952).
 - [15] R. J. Roark and W. C. Young, *Formulas for Stress and Strain*, (McGraw-Hill Book Company, New York, 1975).
 - [16] For the parameters chosen in our model the difference in angular displacement at the beam ends is always small. In the buckling behaviour of fabrics, however, the local curvature can be very large. With an exact expression it has been shown that, even in the case of very large bending angles, the equilibrium shape remains close to that of a circular arc. See, e.g., K. J. Choi and H. S. Ko, ACM T. Graphic. **21**, 604 (2002).
 - [17] B. R. Seshadri and J. C. Newman Jr., "Analyses of Buckling and Stable Tearing in Thin-Sheet Materials", Technical Memorandum NASA-TM-1998-208428, Langley Research Center, Hampton, Virginia (1998).
 - [18] P. Kuhn and I. E. Figge, "Unified Notch-Strength Analysis for Wrought Aluminum", Technical Note NASA-TN-D-1259, Langley Research Center, Hampton, Virginia (1962).